THE JOURNAL OF PHYSICAL CHEMISTRY LETTERS
A JOURNAL OF THE AMERICAN CHEMICAL SOCIETY

pubs.acs.org/JPCL

Letter

The Role of Amide-π Stacking in Resolving the DMF-Benzene Miscibility Paradox

Zhi-Ying Zhao, Ting Chen, Kang Zhou, Peifeng Su, Zhaoxiong Xie, You-Gui Huang,* Lingyi Meng,* Zi-Ang Nan,* and Can-Zhong Lu*

Cite This: *J. Phys. Chem. Lett.* 2025, 16, 11064−11073

Read Online

ACCESS | Metrics & More | Article Recommendations | Supporting Information

ABSTRACT: The complete miscibility of polar *N,N*-dimethylformamide (DMF) with nonpolar benzene (PhH) challenges the classic "like-dissolves-like" principle, highlighting the need for a molecular-level understanding. By synergistically combining multiple research methods, we identified amide-π interactions as the pivotal driving force of this miscibility. First-principles calculations revealed a near-parallel DMF-PhH alignment resembling biological motifs. Meanwhile, the interaction energy of this amide-π stacking was intermediate between those of PhH-PhH (π-π stacking) and water−water (hydrogen bonding) systems. Energy decomposition analysis quantitatively indicated the hybrid nature of amide-π interactions arising from a combination of correlation/dispersion and electrostatics forces. We further demonstrated this interaction's structural dominance and generality through statistical analysis of the Cambridge Structural Database. This work not only resolves the DMF-PhH miscibility paradox but also establishes amide-π interactions as a universal solvation mechanism, providing theoretical guidance for the rational solvent screening in synthetic chemistry.

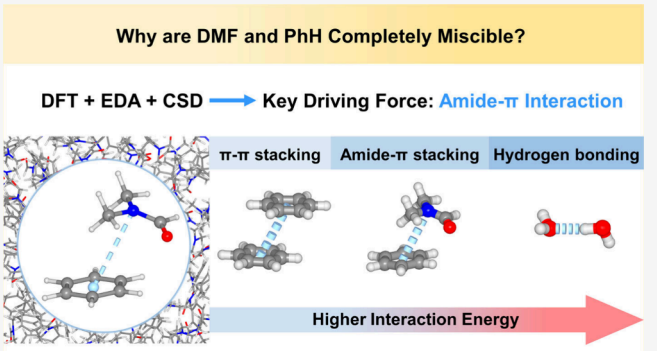

The apparent violation of the conventional "like-dissolves-like" principle in the complete miscibility between nonpolar benzene (PhH) and polar solvents like methanol (CH_3OH) and *N,N*-dimethylformamide (DMF, a common solvent) demands critical further investigations of miscibility mechanisms.[1] According to existing knowledge, traditional miscibility models (Figures 1 (a-c)) emphasize polarity matching through dominant interactions. For example, polar molecules like water (H_2O) and CH_3OH are fully miscible due to hydrogen bonding; nonpolar PhH and toluene ($PhCH_3$) mix completely, owing to shared London dispersion forces and π-π interactions between aromatic rings (ARs). In contrast, H_2O and PhH are immiscible because of incompatible polarities and intermolecular interactions. However, the above-mentioned PhH-polar solvent combinations reveal limitations in conventional wisdom. Recent studies have partially resolved this paradox for CH_3OH-PhH miscibility through identification of unconventional O−H···π and C−H···O hydrogen bonds (Figure 1 (d)).[2] These cooperative interactions provide sufficient stabilization energy to overcome the polarity mismatch. Regrettably, this mechanism fails to extend to the DMF-PhH system due to steric constraints and the absence of protic hydrogens. This unresolved contradiction exposes critical gaps in our understanding of solvation thermodynamics, particularly regarding how nonpolar aromatic systems stabilize polar aprotic solvents through alternative interaction networks.

Emerging evidence from structural biology demonstrates that amide-π stacking interactions serve as a critical driving force in both protein architecture and ligand-binding processes.[3−8] Notably, the amide bond in DMF and the π-system in PhH mirror these biological interaction pairs. Consequently, it is rational to hypothesize that the complete miscibility of DMF and PhH is due to the presence of an amide-π interaction between them. But previous studies have almost exclusively focused on macromolecular systems,[9,10] with scant attention to small-molecule analogues despite their prevalence in synthetic chemistry. Therefore, it is essential to explore the mode and mechanism of the amide-π interaction between small molecules. Herein, we systematically investigated the amide-π interaction in the DMF-PhH system using a range of theoretical methods (Figure 2).

For intermolecular interactions, π-π stacking and hydrogen bonding are highly representative types besides amide-π stacking.[11,12] Therefore, the PhH-PhH (two benzene molecules) and H_2O-H_2O (two water molecules) systems were

Received: September 10, 2025
Revised: October 7, 2025
Accepted: October 10, 2025

https://doi.org/10.1021/acs.jpclett.5c02817
J. Phys. Chem. Lett. 2025, 16, 11064−11073

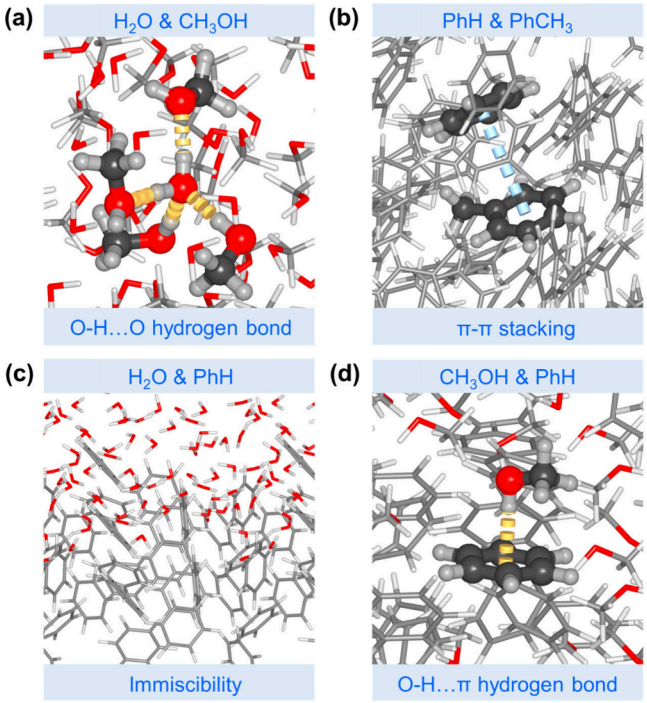

Figure 1. Existing miscibility mechanisms in different systems. (a) H_2O and CH_3OH, (b) PhH and $PhCH_3$, (c) H_2O and PhH, and (d) CH_3OH and PhH.

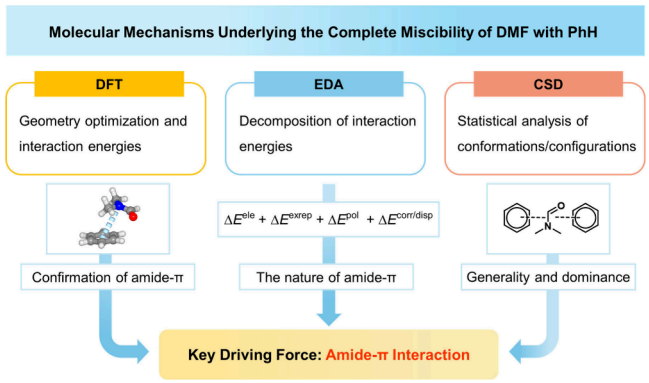

Figure 2. Overview of the research approach and analytical workflow.

selected as references to identify a suitable computational method. The interaction energies (E(interaction)) of these three systems (DMF-PhH, PhH-PhH and H_2O-H_2O) were investigated using different computational methods in this study, such as MP2, CCSD, CCSD(T), and DFT (including different functionals) methods. In Figure 3 (a) and Table S1, it could be seen that the E(interaction) of the DMF-PhH system (amide-π stacking) exceeded that of the PhH-PhH system (π-π stacking) while being slightly lower than that of the H_2O-H_2O system (hydrogen bonding). Literature reports indicated E(interaction) of approximately −2 ∼ −3 kcal/mol for the PhH-PhH system[13,14] and −4.5 ∼ −5.5 kcal/mol for the H_2O-H_2O system,[15,16] consistent with our computational results. Similarly, the E(interaction) for amide-π stacking systems structurally analogous to DMF-PhH, such as formamide-PhH and *N*-methylacetamide-PhH, were about −3.6 ∼ −4.7 kcal/mol,[9,10,17] also aligning closely with our calculated values. Additionally, the absolute interaction energy differences (E(abs diff)) between each method and the CCSD(T) reference

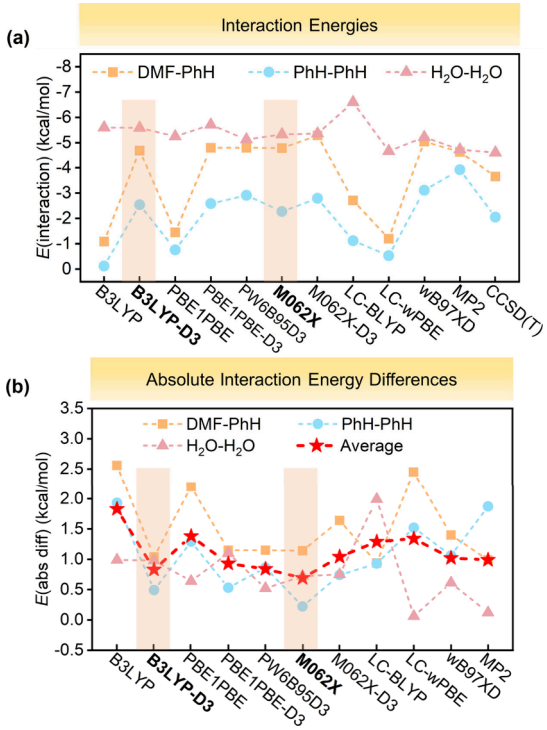

Figure 3. Comparison of interaction energies calculated by different methods. (a) E(interaction) calculated by MP2, CCSD(T), and DFT (including different functionals) methods. (b) Absolute interaction energy differences (E(abs diff) = |corresponding method − CCSD(T)|) obtained from MP2 and DFT (including different functionals) methods. The mean absolute differences across three systems were marked as "Average".

revealed that the M062X (E(interaction) = −4.79 kcal/mol) and B3LYP-D3 (E(interaction) = −4.69 kcal/mol) functionals displayed the smallest E(abs diff, Average) values, demonstrating their superior accuracy compared to other functionals (Figure 3 (b) and Table S2).

In addition to interaction energies, we presented geometrically optimized structures from two functionals (M062X and B3LYP-D3) and the CCSD method in Figures 4 (a-f) and Figures S1 (a-c). For the DMF-PhH system, the angle between the plane of three carbon atoms in DMF and the plane of PhH was about 17° ∼ 19°, and the distance between the nitrogen atom in DMF and the centroid of PhH was about 3.7 Å ∼ 3.9 Å. As expected, they closely resembled the structure of amide-π interaction in proteins reported earlier (Figure S2).[18,19] Similarly, our computed structures for PhH-PhH and H_2O-H_2O systems were also consistent with the geometries of π-π stacking and hydrogen bonding reported in the literature.[14,20,21] Moreover, the differences between the structures optimized by two functionals (M062X and B3LYP-D3) and those optimized by the CCSD method were also evaluated through the root-mean-square deviation (RMSD). As shown in Figures 4 (g-i) and Figures S1 (d-f), RMSD values for all three systems were no more than 1 Å. This indicated that the structures optimized by M062X and B3LYP-D3 functionals were both in excellent agreement with the results of CCSD method.[22]

Based on the above results, it could be concluded that the M062X and B3LYP-D3 functionals were suitable for analyzing the amide-π interaction in terms of both energy and geometrical structure. Due to the high computational cost

https://doi.org/10.1021/acs.jpclett.5c02817
J. Phys. Chem. Lett. 2025, 16, 11064−11073

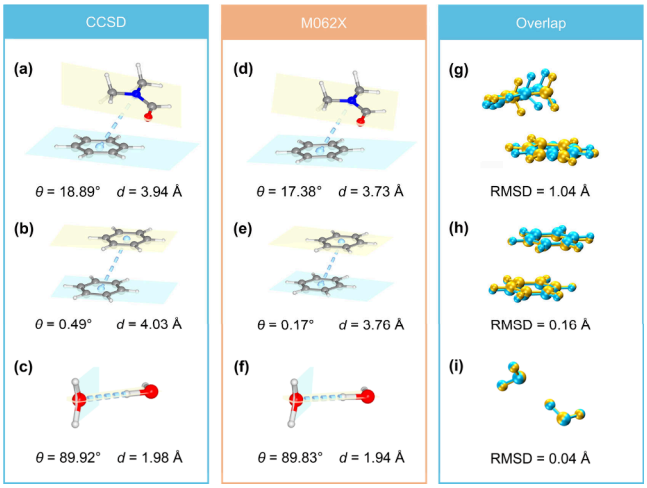

Figure 4. Structures optimized by the CCSD method and M062X functional. Optimized by CCSD: (a) DMF-PhH, (b) PhH-PhH, (c) H_2O-H_2O; Optimized by M062X: (d) DMF-PhH, (e) PhH-PhH, (f) H_2O-H_2O. Overlap between structures optimized by CCSD and M062X (blue: CCSD; gold: M062X): (g) DMF-PhH, (h) PhH-PhH, (i) H_2O-H_2O.

and time requirements of CCSD and CCSD(T) methods, M062X and B3LYP-D3 functionals were selected for further computation in the subsequent study.

With the reliability of the M062X functional for describing the amide-π interaction established, the focus shifted to elucidating how this molecular-level phenomenon translates into the macroscopic miscibility of DMF and PhH from a thermodynamic perspective. To bridge the molecular parameters with bulk miscibility, a simplified thermodynamic model based on the M062X-calculated E(interaction) was constructed: DMF-DMF (−5.84 kcal/mol, Figure S3), PhH-PhH (−2.27 kcal/mol), and DMF-PhH (−4.79 kcal/mol). The energy change (ΔE) for the model reaction $DMF_2 + PhH_2 \rightarrow$ 2 DMF-PhH was calculated to be −1.47 kcal/mol. This exothermic value indicated that the formation of heteromolecular amide-π stacking from the homomolecular liquid is energetically favorable. Considering that the mixing of liquids is typically accompanied by a significant entropy increase, the overall Gibbs free energy change (ΔG) for the miscibility process is negative. This analysis demonstrated that the miscibility of DMF and PhH is a thermodynamically spontaneous process, thereby directly linking the molecular interaction parameter (amide-π stacking energy) to the macroscopic phenomenon of complete miscibility.

Generalized Kohn−Sham energy decomposition analysis (GKS-EDA) based on KS-DFT calculations can provide deeper insights into various chemical problems or phenomena.[23] In this study, XEDA (Xiamen Energy Decomposition Analysis) software[24] was employed to perform GKS-EDA calculations to investigate the nature of the amide-π interaction in detail. The GKS-EDA results by the M062X functional, comprising four terms—an electrostatic term (ΔE^{ele}), exchange-repulsion term (ΔE^{exrep}), polarization term (ΔE^{pol}), and correlation/dispersion term ($\Delta E^{corr/disp}$)—were presented in Figure 5(a), with corresponding numeric values in Table S3. Since the ΔE^{exrep} values showed no significant differences across three systems, the following discussion mainly focused on three attractive terms (ΔE^{ele}, ΔE^{pol}, and $\Delta E^{corr/disp}$), and their respective percentage contributions were quantified for each system. It is well-known that the interaction in the H_2O-H_2O system (Figure 5(b)) was the hydrogen bond, and the essence of the hydrogen bond was electrostatic interaction. Accordingly, ΔE^{ele}(H_2O-H_2O) contributed the most (67%) to the total interaction energy, and its value was also the largest among these three systems. In contrast, the directionality of hydrogen bonds restricted the spatial overlap region of electron clouds, and the relatively low polarizability of H_2O (compared to π-systems like PhH) further weakened the correlation/dispersion energy.[25] These factors collectively resulted in $\Delta E^{corr/disp}$(H_2O-H_2O) contributing the least (13.6%), with its value being the smallest among the three systems. Furthermore, the interaction in the PhH-PhH system (Figure 5(c)) was primarily governed by π-π stacking, and the relatively high polarizability of PhH led to a dominant contribution of $\Delta E^{corr/disp}$(PhH-PhH) (68.9%) to the total interaction energy. This reflected the central role of correlation/dispersion forces in long-range weak interactions, which aligned with the classical theories of graphene interlayer interactions and aromatic stacking.[26] While the proportion of ΔE^{ele}(PhH-PhH) remained relatively small (20.5%), this reduced contribution served to minimize the adverse effects of electrostatic repulsion on π-π stacking configurations, thereby stabilizing the nonpolar-dominated interaction framework.[27] For the DMF-PhH system (amide-π stacking, Figure 5(d)), the contribution of $\Delta E^{corr/disp}$(DMF-PhH) was notably significant (59.7%) and exhibited the largest value among the three systems, highlighting the synergistic effect between correlation/dispersion forces and partial charge transfer.[28]

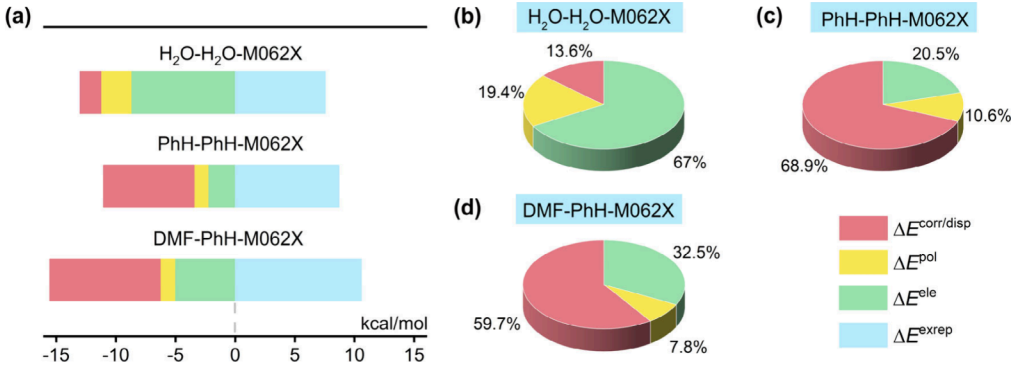

Figure 5. The results of GKS-EDA by the M062X functional. (a) GKS-EDA energy terms for different systems. (b) Percentage contributions of each term in H_2O-H_2O. (c) Percentage contributions of each term in PhH-PhH. (d) Percentage contributions of each term in DMF-PhH.

https://doi.org/10.1021/acs.jpclett.5c02817
J. Phys. Chem. Lett. 2025, 16, 11064−11073

Meanwhile, the value of ΔE^{ele}(DMF-PhH) (32.5%) was between those of ΔE^{ele}(H_2O-H_2O) and ΔE^{ele}(PhH-PhH). This originated from the polarization effect induced by the interaction between the lone pair electrons of the amide group and the π-electron cloud,[29] forming a hybrid correlation/dispersion-electrostatics binding mode. These results provide a molecular-level explanation for the enhanced solubility of aromatic compounds in amide solvents. Since the interactions in these three systems were all intermolecular interactions, which typically involved insignificant charge transfer or electron density redistribution, the induced polarization effects were minimal (as reflected by the small ΔE^{pol} values).[30] However, hydrogen bonds presented partial covalent character due to the strong polarity of H_2O, leading to higher polarization energy (19.4%) compared to pure π-π (10.6%) or amide-π systems (7.8%).[31] Moreover, it was noteworthy that the GKS-EDA results obtained by the B3LYP-D3 functional were very similar (Figure S4 and Table S4).

Besides PhH, our investigations into amide-π interactions have been extended to other 58 aromatic compounds, including biologically relevant molecules, heterocyclic compounds, substituted benzene derivatives, and polycyclic aromatic hydrocarbons. The structure optimizations and interaction energy calculations between DMF and these compounds were studied, respectively (Tables S5−S10: M062X functional; Tables S11−S16: B3LYP-D3 functional). We measured two geometric parameters: the distance (d) between the nitrogen atom of DMF and the centroid of the aromatic ring, and the angle (θ) between the plane of the three carbon atoms in DMF and the plane of the aromatic ring. The geometric parameters, corresponding E(interaction), and whether amide-π stacking formed were listed in Table 1 and Table 2. According to computational results, it was observed that most aromatic compounds could form amide-π stacking with DMF, where the interactions were jointly influenced by the electronic properties and geometric features of the aromatic systems. To be exact, compounds with smaller steric hindrance around aromatic/heteroaromatic rings or those with more abundant delocalized π-electrons were more prone to achieve parallel alignment with DMF, favoring the formation of amide-π interactions. Conversely, hydrogen bonding tended to be the dominant interaction mode. For instance, adjacent methyl groups in *o*-xylene sterically hinder parallel alignment with DMF, favoring hydrogen bonding. On the contrary, minimal steric hindrance in *m*/*p*-xylene enabled effective amide-π stacking with the amide group of DMF (Figures 6 (a-c) and Figures S5 (a-c)). Additionally, positively charged benzimidazolium, with reduced π-electron delocalization, thereby led to hydrogen bonds with DMF, whereas neutral benzimidazole and deprotonated benzimidazolide engaged in amide-π interactions (Figures 6 (d-f) and Figures S5 (d-f)). Mackenzie et al. also discovered that amide-π interactions between AF9 and acyllysines were electrostatically tunable, and electron-rich rings were more conducive to form these interactions,[32] which shared striking parallels with our findings.

To further verify the results of DFT calculation and explore the generality of amide-π interactions, a statistical analysis of crystal structures reported in the Cambridge Structural Database (CSD) was conducted.[33] We focused on systems containing DMF molecules and six-membered aromatic rings, which yielded 3,721 structures, covering 6,319 DMF-AR interaction fragments. This large sample size provided a solid statistical foundation for our analysis. There were two key

Table 1. Geometric Parameters and E(interaction) between DMF and Other Aromatic Compounds (Substituted Benzene Derivatives and Polycyclic Aromatic Hydrocarbons) Using the M062X Functional

Name	d/Å	θ/°	E(interaction)/(kcal/mol)	Amide-π stacking
Benzene	3.73	17.38	−4.79	yes
Toluene	3.68	13.64	−6.80	yes
Aniline	3.72	18.83	−8.12	yes
Nitrobenzene	3.38	12.43	−4.41	yes
o-Xylene	4.31	86.54	−4.02	no
m-Xylene	3.67	14.59	−6.88	yes
p-Xylene	3.67	13.56	−6.84	yes
Fluorobenzene	5.45	89.99	−3.24	no
Chlorobenzene	3.28	6.95	−5.08	yes
Anisole	3.26	7.76	−4.68	yes
Benzenaminium	5.84	66.97	−30.22	no
Phenol	3.67	23.38	−10.99	yes
Phenolate	4.04	38.22	−13.11	no
Benzoate	4.12	22.07	−13.43	no
Phenylmethanol	3.33	5.74	−6.19	yes
Benzaldehyde	3.39	16.19	−5.67	yes
Benzoic acid	3.39	13.82	−5.49	yes
Methyl benzoate	3.78	7.85	−7.53	yes
Naphthalene[a]	3.28	4.16	−6.60	yes
Anthracene[a]	3.24	4.63	−6.34	yes
Phenanthrene[a]	3.18	8.57	−7.72	yes
Pyrene[a]	3.18	9.29	−8.07	yes
Perylene[a]	3.16	7.22	−7.98	yes

[a]Distance to the nearest six-membered aromatic ring.

geometric parameters systematically examined: the distance (d) between the nitrogen atom of DMF and the centroid of the aromatic ring, and the angle (θ) between the plane of three carbon atoms in DMF and the plane of aromatic ring. The statistical results were presented in the heat map shown in Figure 7 (a). Here, the color of each grid represents the fragment numbers (i.e., structural density), as indicated by the vertical axis on the right. A distinct red grid area highlighted the region with the highest structural density, which contained 106 fragments. The characteristic geometric parameters for this region were: θ = 4.30° ∼ 8.60° and d = 3.83 Å ∼ 3.90 Å. Figures 7 (b-c) illustrated the crystal structure fragments of typical DMF-π stacking conformations in this region.[34,35] This heat map could be interpreted as a potential energy surface in an alternative context, while the red region corresponded to the potential energy minimum. It was worth noting that the d values in this hotspot closely matched the structure of amide-π stacking obtained from our previous quantum calculations for the DMF-PhH system. However, the θ values in this region were significantly smaller than those derived from our idealized computational results. Analysis revealed that this discrepancy primarily arose from substituted aromatic rings common in actual crystal structures, where substituents reduced the θ values. Consequently, our structural examination of diverse aromatic systems (Figures S6 and S7) definitively confirmed this trend. We also conducted a statistical analysis of the stacking configurations involving DMF and aromatic systems through amide-π interactions. The detailed structures are shown in Figures 7 (d-f), with corresponding specific examples illustrated in Figure S8. Figure 7 (d) included not only the simple stacking configuration of one DMF with one AR (Type

https://doi.org/10.1021/acs.jpclett.5c02817
J. Phys. Chem. Lett. 2025, 16, 11064−11073

Table 2. Geometric Parameters and *E*(interaction) between DMF and Other Aromatic Compounds (Biologically Relevant Molecules and Heterocyclic Compounds) Using the M062X Functional

Name	*d*/Å	*θ*/°	*E*(interaction)/(kcal/mol)	Amide-*π* Stacking
Benzimidazole[a]	3.78	24.51	−9.25	yes
Benzimidazolide[a]	3.77	4.00	−13.57	yes
Benzimidazolium[a]	4.70	89.99	−16.24	no
Pyrrole	3.33	17.82	−6.67	yes
Pyrazole	4.06	66.33	−9.83	no
Imidazole	3.25	14.84	−7.59	yes
1,2,3-Triazole	4.12	71.08	−11.22	no
2*H*-1,2,3-Triazole	3.22	3.69	−4.30	yes
1,2,4-Triazole	3.56	23.00	−4.33	yes
4*H*-1,2,4-Triazole	3.17	4.08	−9.24	yes
Tetrazole	5.08	15.46	−12.29	no
2*H*-Tetrazole	5.06	28.56	−10.53	no
Furan	3.21	0.88	−4.19	yes
Oxazole	3.20	12.86	−4.59	yes
Isoxazole	3.20	15.26	−5.39	yes
1,2,5-Oxadiazole	3.22	2.78	−6.29	yes
Thiophene	3.73	22.25	−4.90	yes
Thiazole	3.25	5.68	−5.32	yes
Isothiazole	3.66	20.00	−4.94	yes
1,3,4-Thiadiazole	5.68	56.33	−5.28	no
Pyridine	3.23	10.26	−4.56	yes
Pyrazine	3.26	9.08	−4.81	yes
Pyrimidine	3.19	11.78	−3.41	yes
Pyridazine	3.52	9.75	−7.07	yes
1,3,5-Triazine	3.67	4.79	−4.52	yes
1,2,4-Triazine	3.18	7.33	−6.12	yes
1,2,3-Triazine	3.50	7.92	−7.64	yes
9*H*-Purine[a]	3.78	34.31	−10.78	yes
Purin-9-ide[a]	3.17	8.49	−10.80	yes
Adenine[b]	3.65	28.23	−8.63	yes
Adeninide[b]	3.18	7.10	−11.26	yes
2-Aminoadenine[a]	3.14	9.86	−11.49	yes
2-Aminoadeninide	3.10	6.87	−18.18	yes
Cytosine	3.15	11.69	−8.60	yes
Thymine	4.90	72.93	−8.82	no
Uracil	3.15	5.62	−9.23	yes

[a]Distance to the nearest six-membered aromatic ring. [b]Distance to the nearest five-membered aromatic ring.

A)[36] but also sandwich-like structures comprising two ARs with one DMF (Type B),[37] two DMFs with one AR (Type C),[38] and a stacked sequence of AR-DMF-DMF-AR (Type D).[39] Types E, F, and G illustrated amide-*π* stacking configurations incorporating *π*-*π* stacking.[40−42] Owing to the long-range order in crystals, we also identified amide-*π* configurations exhibiting infinite stacking of DMF with ARs along specific directions (Types H).[43] These DMF-AR stacking configurations might potentially correspond to structural motifs in completely miscible DMF-PhH solutions. Furthermore, the oxygen atom of DMF could be a hydrogen-bond acceptor or a coordination atom. As a result, amide-*π* stacking interactions could also act cooperatively with hydrogen bonds (Figure 7 (e), Types I−O)[44−50] and coordination bonds (Figure 7 (f), Types P−V).[51−57] In conclusion, this large-scale CSD analysis provided compelling evidence that amide-*π* interactions exhibited high generality and structural dominance not only in DMF-PhH but also extensively across crystalline DMF-six-membered aromatic ring systems.

In summary, our study confirmed that amide-*π* interaction was the key driving force for the anomalous miscibility of polar DMF and nonpolar PhH using a synergistic multimethod approach. First-principles calculations revealed that both the M062X and B3LYP-D3 functionals exhibited excellent agreement with the results obtained from CCSD and CCSD(T) methods. The *E*(interaction) of the DMF-PhH system (amide-*π* stacking) was higher than that of the PhH-PhH system (*π*-*π* stacking) but marginally lower than that of the H_2O-H_2O system (hydrogen bonding). Our results further confirmed that the mixing process between DMF and PhH was thermodynamically favorable. What's more, GKS-EDA quantified the hybrid nature of this interaction, characterized by significant contributions from both correlation/dispersion energy and electrostatic forces. Statistical analysis based on the CSD systematically investigated conformations and configurations of DMF-AR systems, indicating the structural dominance and pronounced generality of amide-*π* interactions. This work establishes amide-*π* interactions as a fundamental and universal solvation mechanism in polar aprotic-nonpolar aromatic systems. While our study provides this fundamental understanding, future molecular dynamics studies will be invaluable for exploring the dynamic solvation structure and transport properties of DMF-aromatic mixtures. These amide-*π* stacking

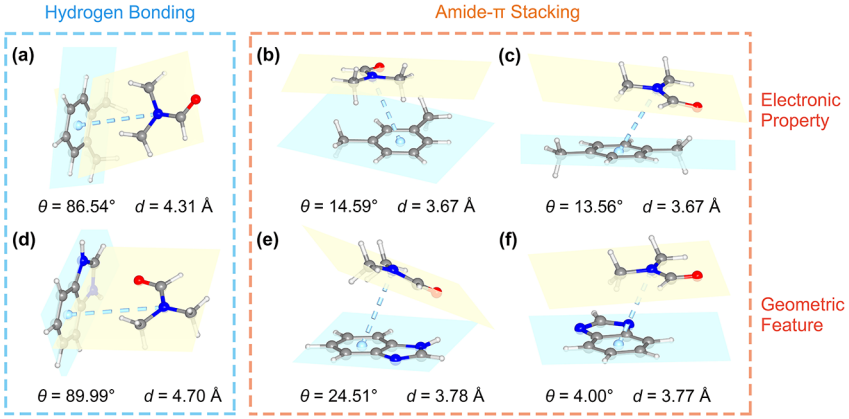

Figure 6. Structures optimized by the M062X functional. (a) DMF-*o*-xylene; (b) DMF-*m*-xylene; (c) DMF-*p*-xylene; (d) DMF-benzimidazolium; (e) DMF-benzimidazole; (f) DMF-benzimidazolide.

https://doi.org/10.1021/acs.jpclett.5c02817
J. Phys. Chem. Lett. 2025, 16, 11064−11073

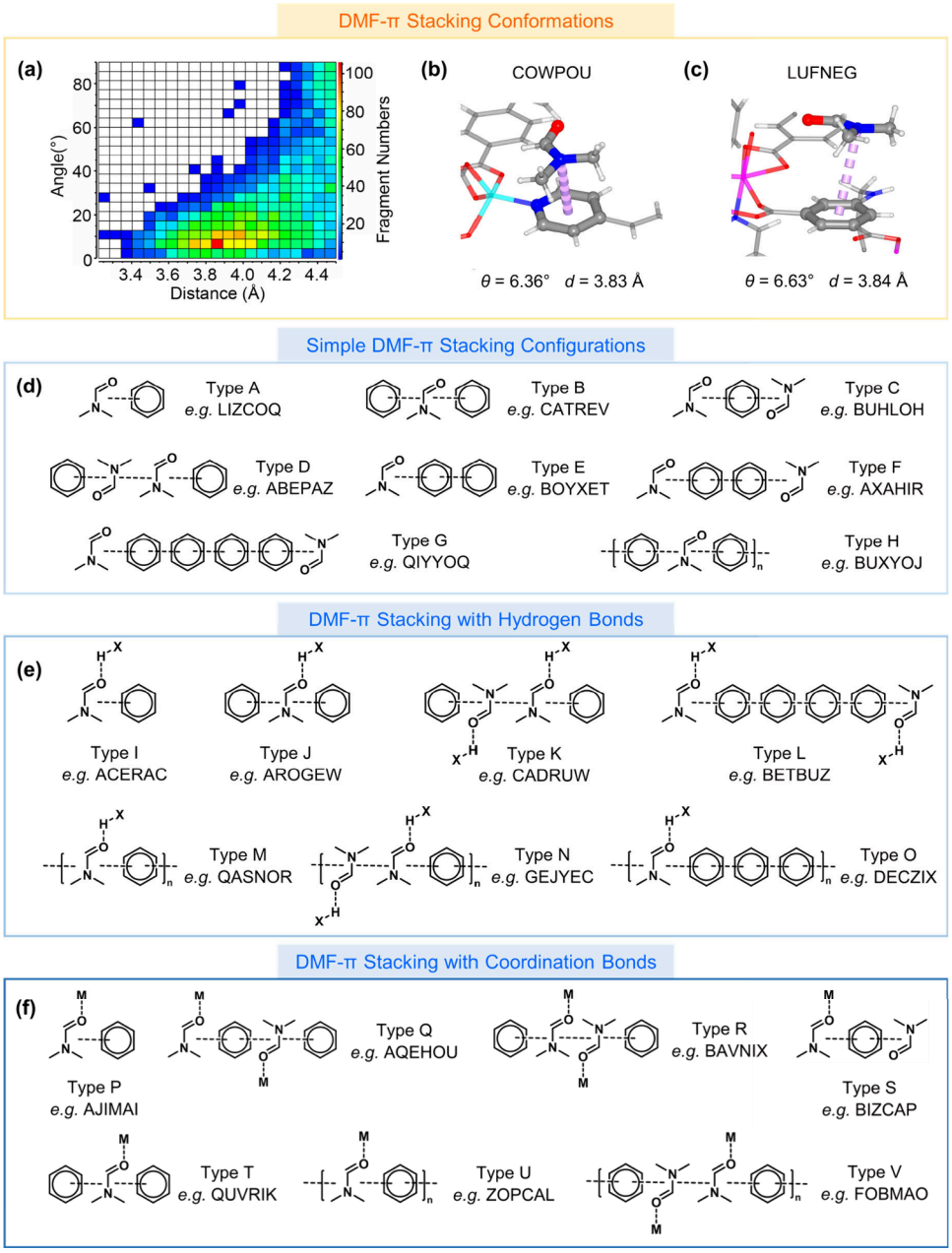

Figure 7. Statistical analysis of crystal structures reported in CSD. (a) Heat map of systems containing DMF and six-membered aromatic rings. (b-c) Typical DMF-π stacking conformations in red region. (d-f) Stacking configurations involving DMF and aromatic systems through amide-π interactions.

interactions could be exploited to guide the design of small-molecule conformations, enable advanced cocrystal engineering, and modulate supramolecular host−guest interactions.

METHODS

First-Principles Calculations. We conducted the geometrical optimizations and the calculations of interaction energies (E(interaction)) using first-principles calculations. The Gaussian 16 program[58] and ma-def2-TZVP basis set[59,60] were used for *ab initio* molecular orbital calculations. For MP2[61] and DFT (including LC-wPBE,[62] LC-BLYP,[63] wB97XD,[64] B3LYP,[65] B3LYP-D3 (B3LYP with EmpiricalDispersion = GD3[66]), M062X,[27] M062X-D3 (M062X with EmpiricalDispersion = GD3), PBE1PBE,[67] PBE1PBE-D3 (PBE1PBE with EmpiricalDispersion = GD3), and PW6B95D3[15] functionals) methods, both structure optimization and interaction energy calculations were performed using the same method. For the structure optimized by CCSD,[68] the interaction energy was calculated using CCSD(T).[69] The full names of the technical abbreviations were provided in the Supporting Information.

The basis set superposition error (BSSE) was considered for the dimer energy and corrected using the counterpoise method.[70] The interaction energy between A and B was calculated as follows: E(interaction) = E(A−B, counterpoise corrected energy) − E(A) − E(B).

Energy Decomposition Analysis. The interaction energies calculated by B3LYP-D3 and M062X functionals were decomposed and analyzed using XEDA on the XACS Web site (https://xacs.xmu.edu.cn/). The total interaction

https://doi.org/10.1021/acs.jpclett.5c02817
J. Phys. Chem. Lett. 2025, 16, 11064−11073

energy was divided into the following components: electrostatic energy (ES), exchange energy (EX), repulsion energy (REP), polarization energy (POL), Grimme's dispersion correction energy (DC), and electron correlation energy (CORR). These energy components were integrated to obtain the following four terms: electrostatic term (ΔE^{ele} = ES), exchange-repulsion term (ΔE^{exrep} = EX + REP), polarization term (ΔE^{pol} = POL), and correlation/dispersion term ($\Delta E^{corr/disp}$ = CORR + DC).

Cambridge Structural Database Statistical Analysis. Structural statistics were extracted using Conquest[71] with CSD version 5.45. In order to avoid the interference from abnormal data on statistical results, structures without three-dimensional coordinates were determined and disordered structures were filtered. The heat map was generated with Mercury.[72]

Diamond and Visual Molecular Dynamics. The distances and angles between molecules in optimized structures were calculated using Diamond software (https://www.crystalimpact.de/diamond.). The structures were analyzed using Visual Molecular Dynamics[73] to calculate the root-mean-square deviation (RMSD).

Materials Studio. We obtained the schematic diagram in Figure 1 by performing a simple structural optimization with Materials Studio software (Version 2020; Dassault Systèmes BIOVIA).

■ ASSOCIATED CONTENT

Supporting Information

The Supporting Information is available free of charge at https://pubs.acs.org/doi/10.1021/acs.jpclett.5c02817.

Results of GKS-EDA by B3LYP-D3 functional, the structure optimization and interaction energy calculations between DMF and other aromatic compounds, specific examples of different types involving DMF and aromatic systems (PDF)

Transparent Peer Review report available (PDF)

■ AUTHOR INFORMATION

Corresponding Authors

Can-Zhong Lu − *State Key Laboratory of Structural Chemistry, Fujian Institute of Research on the Structure of Matter, Chinese Academy of Sciences, Fuzhou, Fujian 350002, P.R. China; Xiamen Key Laboratory of Rare Earth Photoelectric Functional Materials, Xiamen Institute of Rare Earth Materials, Haixi Institutes, Chinese Academy of Sciences, Xiamen 361021, P. R. China;* orcid.org/0000-0002-8298-4132; Email: czlu@fjirsm.ac.cn

Zi-Ang Nan − *State Key Laboratory of Structural Chemistry, Fujian Institute of Research on the Structure of Matter, Chinese Academy of Sciences, Fuzhou, Fujian 350002, P.R. China; Xiamen Key Laboratory of Rare Earth Photoelectric Functional Materials, Xiamen Institute of Rare Earth Materials, Haixi Institutes, Chinese Academy of Sciences, Xiamen 361021, P. R. China*; Email: nanziang@fjirsm.ac.cn

Lingyi Meng − *State Key Laboratory of Structural Chemistry, Fujian Institute of Research on the Structure of Matter, Chinese Academy of Sciences, Fuzhou, Fujian 350002, P.R. China; Xiamen Key Laboratory of Rare Earth Photoelectric Functional Materials, Xiamen Institute of Rare Earth Materials, Haixi Institutes, Chinese Academy of Sciences, Xiamen 361021, P. R. China;* orcid.org/0000-0002-8985-5093; Email: lymeng@fjirsm.ac.cn

You-Gui Huang − *State Key Laboratory of Structural Chemistry, Fujian Institute of Research on the Structure of Matter, Chinese Academy of Sciences, Fuzhou, Fujian 350002, P.R. China; Xiamen Key Laboratory of Rare Earth Photoelectric Functional Materials, Xiamen Institute of Rare Earth Materials, Haixi Institutes, Chinese Academy of Sciences, Xiamen 361021, P. R. China;* orcid.org/0000-0001-9962-3723; Email: yghuang@fjirsm.ac.cn

Authors

Zhi-Ying Zhao − *State Key Laboratory of Structural Chemistry, Fujian Institute of Research on the Structure of Matter, Chinese Academy of Sciences, Fuzhou, Fujian 350002, P.R. China; Xiamen Key Laboratory of Rare Earth Photoelectric Functional Materials, Xiamen Institute of Rare Earth Materials, Haixi Institutes, Chinese Academy of Sciences, Xiamen 361021, P. R. China*

Ting Chen − *State Key Laboratory of Structural Chemistry, Fujian Institute of Research on the Structure of Matter, Chinese Academy of Sciences, Fuzhou, Fujian 350002, P.R. China; Xiamen Key Laboratory of Rare Earth Photoelectric Functional Materials, Xiamen Institute of Rare Earth Materials, Haixi Institutes, Chinese Academy of Sciences, Xiamen 361021, P. R. China*

Kang Zhou − *State Key Laboratory for Physical Chemistry of Solid Surfaces, Collaborative Innovation Center of Chemistry for Energy Materials, Fujian Provincial Key Laboratory of Theoretical and Computational Chemistry, Department of Chemistry, College of Chemistry and Chemical Engineering, Xiamen University, Xiamen 361005, China*

Peifeng Su − *State Key Laboratory for Physical Chemistry of Solid Surfaces, Collaborative Innovation Center of Chemistry for Energy Materials, Fujian Provincial Key Laboratory of Theoretical and Computational Chemistry, Department of Chemistry, College of Chemistry and Chemical Engineering, Xiamen University, Xiamen 361005, China;* orcid.org/0000-0003-4398-6888

Zhaoxiong Xie − *State Key Laboratory for Physical Chemistry of Solid Surfaces, Collaborative Innovation Center of Chemistry for Energy Materials, Fujian Provincial Key Laboratory of Theoretical and Computational Chemistry, Department of Chemistry, College of Chemistry and Chemical Engineering, Xiamen University, Xiamen 361005, China;* orcid.org/0000-0002-4225-6536

Complete contact information is available at: https://pubs.acs.org/10.1021/acs.jpclett.5c02817

Notes

The authors declare no competing financial interest.

■ ACKNOWLEDGMENTS

We gratefully acknowledge the support from the National Key R&D Program of China (Grant No. 2021YFB3500400 (L.M.)), the Self-deployment Project Research Program of Haixi Institutes, Chinese Academy of Sciences (Grant No. CXZX-2022-GH02 (L.M.)), the National Science Foundation of China (Grant Nos. 52073286 and 22275185 (C.-Z.L.)), the Natural Science Foundation of Fujian Province (2023J01215 (L.M.)), the Supporting Project of Fujian Province for "Science and Technology Service Network Initiative, CAS" (2023T3024 (L.M.)), the XMIREM Autonomously Deployment Project (2023GG01 (C.-Z.L.)), Fujian Science & Technology Innovation Laboratory for Optoelectronic In-

formation of China (2021ZZ115 (C.-Z.L.)), and Opening Foundation of State Key Laboratory of Physical Chemistry of Solid Surfaces, Xiamen University (202419 (L.M.) and 202426 (Z.-A.N.)).

REFERENCES

(1) Sadek, P. C. The HPLC Solvent Guide, 2nd ed.; Wiley, 2002.
(2) Di Mino, C.; Seel, A. G.; Clancy, A. J.; Headen, T. F.; Földes, T.; Rosta, E.; Sella, A.; Skipper, N. T. Strong structuring arising from weak cooperative O-H···π and C-H···O hydrogen bonding in benzene-methanol solution. *Nat. Commun.* **2023**, *14* (1), 5900.
(3) Davis, M. I.; Bennett, M. J.; Thomas, L. M.; Bjorkman, P. J. Crystal structure of prostate-specific membrane antigen, a tumor marker and peptidase. *Proc. Nat. Acad. Sci.* **2005**, *102* (17), 5981−5986.
(4) Alleyne, C.; Amin, R. P.; Bhatt, B.; Bianchi, E.; Blain, J. C.; Boyer, N.; Branca, D.; Embrey, M. W.; Ha, S. N.; Jette, K.; Johns, D. G.; Kerekes, A. D.; Koeplinger, K. A.; LaPlaca, D.; Li, N.; Murphy, B.; Orth, P.; Ricardo, A.; Salowe, S.; Seyb, K.; Shahripour, A.; Stringer, J. R.; Sun, Y.; Tracy, R.; Wu, C.; Xiong, Y.; Youm, H.; Zokian, H. J.; Tucker, T. J. Series of Novel and Highly Potent Cyclic Peptide PCSK9 Inhibitors Derived from an mRNA Display Screen and Optimized via Structure-Based Design. *J. Med. Chem.* **2020**, *63* (22), 13796−13824.
(5) Takemoto, Y.; Ito, A.; Niwa, H.; Okamura, M.; Fujiwara, T.; Hirano, T.; Handa, N.; Umehara, T.; Sonoda, T.; Ogawa, K.; Tariq, M.; Nishino, N.; Dan, S.; Kagechika, H.; Yamori, T.; Yokoyama, S.; Yoshida, M. Identification of Cyproheptadine as an Inhibitor of SET Domain Containing Lysine Methyltransferase 7/9 (Set7/9) That Regulates Estrogen-Dependent Transcription. *J. Med. Chem.* **2016**, *59* (8), 3650−3660.
(6) Ferreira de Freitas, R.; Schapira, M. A systematic analysis of atomic protein-ligand interactions in the PDB. *MedChemComm* **2017**, *8* (10), 1970−1981.
(7) Ye, S.; Zhong, K.; Huang, Y.; Zhang, G.; Sun, C.; Jiang, J. Artificial Intelligence-based Amide-II Infrared Spectroscopy Simulation for Monitoring Protein Hydrogen Bonding Dynamics. *J. Am. Chem. Soc.* **2024**, *146* (4), 2663−2672.
(8) Walker, D. R.; Alizadehmojarad, A. A.; Kolomeisky, A. B.; Hartgerink, J. D. Charge-Free, Stabilizing Amide-π Interactions Can Be Used to Control Collagen Triple-Helix Self-Assembly. *Biomacromolecules* **2021**, *22* (5), 2137−2147.
(9) Bootsma, A. N.; Wheeler, S. E. Stacking Interactions of Heterocyclic Drug Fragments with Protein Amide Backbones. *ChemMedChem.* **2018**, *13* (8), 835−841.
(10) Harder, M.; Kuhn, B.; Diederich, F. Efficient Stacking on Protein Amide Fragments. *ChemMedChem.* **2013**, *8* (3), 397−404.
(11) Calinsky, R.; Levy, Y. Histidine in Proteins: pH-Dependent Interplay between π-π, Cation-π, and CH-π Interactions. *J. Chem. Theory Comput.* **2024**, *20* (15), 6930−6945.
(12) Řezáč, J. Non-Covalent Interactions Atlas Benchmark Data Sets: Hydrogen Bonding. *J. Chem. Theory Comput.* **2020**, *16* (4), 2355−2368.
(13) Sinnokrot, M. O.; Valeev, E. F.; Sherrill, C. D. Estimates of the Ab Initio Limit for π-π Interactions: The Benzene Dimer. *J. Am. Chem. Soc.* **2002**, *124* (36), 10887−10893.
(14) Sinnokrot, M. O.; Sherrill, C. D. High-Accuracy Quantum Mechanical Studies of π-π Interactions in Benzene Dimers. *J. Phys. Chem. A* **2006**, *110* (37), 10656−10668.
(15) Zhao, Y.; Truhlar, D. G. Design of Density Functionals That Are Broadly Accurate for Thermochemistry, Thermochemical Kinetics, and Nonbonded Interactions. *J. Phys. Chem. A* **2005**, *109* (25), 5656−5667.
(16) Boese, A. D.; Martin, J. M. L. Development of density functionals for thermochemical kinetics. *J. Chem. Phys.* **2004**, *121* (8), 3405−3416.
(17) Imai, Y. N.; Inoue, Y.; Nakanishi, I.; Kitaura, K. Amide-π interactions between formamide and benzene. *J. Comput. Chem.* **2009**, *30* (14), 2267−2276.
(18) Marek, M.; Shaik, T. B.; Heimburg, T.; Chakrabarti, A.; Lancelot, J.; Ramos-Morales, E.; Da Veiga, C.; Kalinin, D.; Melesina, J.; Robaa, D.; Schmidtkunz, K.; Suzuki, T.; Holl, R.; Ennifar, E.; Pierce, R. J.; Jung, M.; Sippl, W.; Romier, C. Characterization of Histone Deacetylase 8 (HDAC8) Selective Inhibition Reveals Specific Active Site Structural and Functional Determinants. *J. Med. Chem.* **2018**, *61* (22), 10000−10016.
(19) Ahmed-Belkacem, A.; Colliandre, L.; Ahnou, N.; Nevers, Q.; Gelin, M.; Bessin, Y.; Brillet, R.; Cala, O.; Douguet, D.; Bourguet, W.; Krimm, I.; Pawlotsky, J.-M.; Guichou, J.-F. Fragment-based discovery of a new family of non-peptidic small-molecule cyclophilin inhibitors with potent antiviral activities. *Nat. Commun.* **2016**, *7* (1), 12777.
(20) Wheeler, S. E. Revisiting the Hunter-Sanders Model for π-π Interactions. *J. Am. Chem. Soc.* **2025**, *147* (23), 19738−19750.
(21) Xantheas, S. S.; Dunning, T. H., Jr. Ab initio studies of cyclic water clusters (H2O)n, n = 1−6. I. Optimal structures and vibrational spectra. *J. Chem. Phys.* **1993**, *99* (11), 8774−8792.
(22) Mukherjee, S.; Balius, T. E.; Rizzo, R. C. Docking Validation Resources: Protein Family and Ligand Flexibility Experiments. *J. Chem. Inf. Model.* **2010**, *50* (11), 1986−2000.
(23) Su, P.; Jiang, Z.; Chen, Z.; Wu, W. Energy Decomposition Scheme Based on the Generalized Kohn-Sham Scheme. *J. Phys. Chem. A* **2014**, *118* (13), 2531−2542.
(24) Tang, Z.; Song, Y.; Zhang, S.; Wang, W.; Xu, Y.; Wu, D.; Wu, W.; Su, P. XEDA, a fast and multipurpose energy decomposition analysis program. *J. Comput. Chem.* **2021**, *42* (32), 2341−2351.
(25) London, F. The general theory of molecular forces. *Trans. Faraday Soc.* **1937**, *33* (0), 8b−26.
(26) Sherrill, C. D. Energy Component Analysis of π Interactions. *Acc. Chem. Res.* **2013**, *46* (4), 1020−1028.
(27) Zhao, Y.; Truhlar, D. G. The M06 suite of density functionals for main group thermochemistry, thermochemical kinetics, noncovalent interactions, excited states, and transition elements: two new functionals and systematic testing of four M06-class functionals and 12 other functionals. *Theor. Chem. Acc.* **2008**, *120* (1), 215−241.
(28) Fu, Z.; Qiao, J.-W.; Cui, F.-Z.; Zhang, W.-Q.; Wang, L.-H.; Lu, P.; Yin, H.; Du, X.-Y.; Qin, W.; Hao, X.-T. π-π Stacking Modulation via Polymer Adsorption for Elongated Exciton Diffusion in High-Efficiency Thick-Film Organic Solar Cells. *Adv. Mater.* **2024**, *36* (21), 2313532.
(29) Wang, Y.; Zhu, X.; Han, J.; Liang, T.; Wu, N.; Xiang, J.; Ouyang, G.; Liu, M. Light-Up Fluorescence and Circularly Polarized Luminescence in Achiral Interlocked Framework via Adaptive Lone Pair-π Interaction Confinement. *Adv. Sci.* **2024**, *11* (40), 2406890.
(30) Kumar, N.; Saha, S.; Sastry, G. N. Towards developing a criterion to characterize non-covalent bonds: a quantum mechanical study. *Phys. Chem. Chem. Phys.* **2021**, *23* (14), 8478−8488.
(31) Rozas, I.; Alkorta, I.; Elguero, J. Behavior of Ylides Containing N, O, and C Atoms as Hydrogen Bond Acceptors. *J. Am. Chem. Soc.* **2000**, *122* (45), 11154−11161.
(32) Krone, M. W.; Travis, C. R.; Lee, G. Y.; Eckvahl, H. J.; Houk, K. N.; Waters, M. L. More Than π-π-π Stacking: Contribution of Amide-π and CH-π Interactions to Crotonyllysine Binding by the AF9 YEATS Domain. *J. Am. Chem. Soc.* **2020**, *142* (40), 17048−17056.
(33) Allen, F. The Cambridge Structural Database: a quarter of a million crystal structures and rising. *Acta Crystallogr. Sect. B* **2002**, *58* (3), 380−388.
(34) Lan, A.; Li, K.; Wu, H.; Olson, D. H.; Emge, T. J.; Ki, W.; Hong, M.; Li, J. A Luminescent Microporous Metal-Organic Framework for the Fast and Reversible Detection of High Explosives. *Angew. Chem., Int. Ed.* **2009**, *48* (13), 2334−2338.
(35) Das, M. C.; Bharadwaj, P. K. A Porous Coordination Polymer Exhibiting Reversible Single-Crystal to Single-Crystal Substitution Reactions at Mn(II) Centers by Nitrile Guest Molecules. *J. Am. Chem. Soc.* **2009**, *131* (31), 10942−10949.

https://doi.org/10.1021/acs.jpclett.5c02817
J. Phys. Chem. Lett. 2025, 16, 11064−11073

(36) Wang, X.; Li, M.; Cao, W.; Li, W.; Gao, H.; Zhang, Q.; Zhou, H.; Zhang, X. Crystal structure, optical properties, mobility, and photoelectric performance of $[PEA]_3[Bi_2I_9]$. *Appl. Organomet. Chem.* **2023**, *37* (11), No. e7245.
(37) He, L.; An, Y.; Yuan, L.; Yamato, K.; Feng, W.; Gerlitz, O.; Zheng, C.; Gong, B. Macrocyclic aromatic tetrasulfonamides with a stable cone conformation. *Chem. Commun.* **2005**, No. 30, 3788−3790.
(38) Lü, J.; Han, L.-W.; Alsmail, N. H.; Blake, A. J.; Lewis, W.; Cao, R.; Schröder, M. Control of Assembly of Dihydropyridyl and Pyridyl Molecules via Directed Hydrogen Bonding. *Cryst. Growth Des.* **2015**, *15* (9), 4219−4224.
(39) Wang, X.; Zeng, Z.; Shi, D.; Wei, X.; Zong, Z. Methyl 2-amino-4-(4-methylphenyl)-5-oxo-5,6-dihydro-4*H*-pyrano[3,2-*c*]quinoline-3-carboxylate dimethylformamide solvate. *Acta Crystallogr. Sect. E* **2004**, *60* (9), o1606−o1608.
(40) Vinh Huynh, H.; Jothibasu, R. Formation of Homoleptic Tetracarbene versus cis-Chelating Dicarbene Complexes of Nickel(II) and Applications in Kumada-Corriu Couplings. *Eur. J. Inorg. Chem.* **2009**, *2009* (13), 1926−1931.
(41) Liu, X.; Shi, D.; Tang, J.; Yang, D.; Li, J. 5′-Methylsulfanyl-4′-oxo-7′-phenyl-3′,4′-dihydro-1′*H*-spiro[cyclohexane-1,2′-quinazoline]-8′-carbonitrile dimethylformamide monosolvate. *Acta Crystallogr. Sect. E* **2011**, *67* (8), o2016.
(42) Meza-Morales, W.; Alvarez-Ricardo, Y.; Pérez-González, L. L.; Tavera-Hernández, R.; Ramírez-Apan, M. T.; Toscano, R. A.; Sánchez-Obregón, R.; Obregón-Mendoza, M. A.; Enríquez, R. G. First Gallium and Indium Crystal Structures of Curcuminoid Homoleptic Complexes: All-Different Ligand Stereochemistry and Cytotoxic Potential. *Int. J. Mol. Sci.* **2023**, *24*, 16324.
(43) Chiboub Fellah, F. Z.; Costes, J.-P.; Duhayon, C.; Daran, J.-C.; Tuchagues, J.-P. Mononuclear Cu and dinuclear Cu-Ln complexes of benzimidazole based ligands including N and O donors: Syntheses, characterization, X-ray molecular structures and magnetic properties. *Polyhedron* **2010**, *29* (9), 2111−2119.
(44) Wu, H.; Bai, Y.; Yuan, J.; Wang, H.; Pan, G.; Yu, G.; Shu, X. Synthesis and DNA-binding Properties of a Cationic Seven-coordinate Manganese(II) Complex Formed with the Tripodal Ligand Tris(Nmethylbenzimidazol- 2-ylmethyl)amine and Salicylate. *Z. Naturforsch. B* **2012**, *67* (8), 819−826.
(45) Zhao, X.-L.; Wang, M.; Geng, J.; Huang, W. Fenton-like reactions for pyrazolone ester based heterocyclic dyes with reversible hydrazone-azo tautomerism. *Polyhedron* **2021**, *202*, 115208.
(46) Tran, N. T.; Min, T.; Franz, A. K. Silanediol Hydrogen Bonding Activation of Carbonyl Compounds. *Chem. - Eur. J.* **2011**, *17* (36), 9897−9900.
(47) Rao, A. R. B.; Pal, S. Regioselective cyclometallation of 4-*R*-1-naphthaldehyde benzoylhydrazones: Palladium(II) complexes with CNO pincer like ligands. *J. Organomet. Chem.* **2013**, *731*, 67−72.
(48) Edkins, K.; Tweedy, J.; Fung, S.; Edkins, R. M. Steric influence on solvate formation-a comparison of resorcylic acid and two brominated derivatives. *CrystEngComm* **2022**, *24* (7), 1368−1376.
(49) Osinski, A. J.; Morris, D. L.; Herrick, R. S.; Ziegler, C. J. $Re(CO)_3$-Templated Synthesis of α-Amidinoazadi(benzopyrro)-methenes. *Inorg. Chem.* **2017**, *56* (24), 14734−14737.
(50) Yamamoto, L. M.; Nunes, J. H. B.; Ribeiro, M. A.; Ferreira, A. M. d. C.; Lustri, W. R.; Corbi, P. P. Copper(II) and silver(I) complexes with sulfamethizole: synthesis, spectroscopic characterization, ESI-QTOF mass spectrometric analysis, crystal structure and antibacterial activities. *Polyhedron* **2017**, *138*, 168−176.
(51) Xie, H.; Meng, S.; Zhu, Y.; Bai, P. {2,2′-[5-Bromopyridine-2,3-diylbis(nitrilomethylidyne)]diphenolato}chlorido-(dimethylformamide)manganese(III). *Acta Crystallogr. Sect. E* **2009**, *65* (12), m1671.
(52) Liu, Y.; Yang, Z.; Zhang, K.; Wu, Y.; Zhu, J.; Zhou, T. Crystal Structures, Antioxidation, and DNA Binding Properties of Sm^{III} Complexes. *Aust. J. Chem.* **2011**, *64* (3), 345−354.
(53) Dinca, A. S.; Ghirri, A.; Madalan, A. M.; Affronte, M.; Andruh, M. Dodecanuclear $[Cu^{II}_6Gd^{III}_6]$ Nanoclusters as Magnetic Refrigerants. *Inorg. Chem.* **2012**, *51* (7), 3935−3937.
(54) Wang, Y.; Liu, Z.; Gao, J.-Y. (3,5-Dichlorosalicylaldehyde thiosemicarbazonato-κ3S, N1, O)(N, N′-dimethylformamide-κO)-copper(II) dimethylformamide solvate. *Acta Crystallogr. Sect. E* **2008**, *64* (5), m633−m634.
(55) Kuang, W.-W.; Zhu, L.-L.; Xu, Y.; Yang, P.-P. A tetranuclear holmium compound exhibiting single molecule magnet behavior. *Inorg. Chem. Commun.* **2015**, *61*, 169−172.
(56) Müller, M.; Buchner, M. R. Solution Behavior of Beryllium Halides in Dimethylformamide. *Inorg. Chem.* **2019**, *58* (19), 13276−13284.
(57) Parsaei, M.; Akhbari, K.; Tylianakis, E.; Froudakis, G. E. Computational Simulation of a Three-Dimensional Mg-based Metal-Organic Framework as Nanoporous Anticancer Drug Carrier. *Cryst. Growth Des.* **2023**, *23* (11), 8396−8406.
(58) Frisch, M. J.; Trucks, G. W.; Schlegel, H. B.; Scuseria, G. E.; Robb, M. A.; Cheeseman, J. R.; Scalmani, G.; Barone, V.; Petersson, G. A.; Nakatsuji, H.; Li, X.; Caricato, M.; Marenich, A. V.; Blolino, J.; Janesko, B. G.; Gomperts, R.; Mennucci, B.; Hratchian, H. P.; Ortiz, J. V.; Izmaylov, A. F.; Sonnenberg, J. L.; Williams-Young, D.; Ding, F.; Lipparini, F.; Egidi, F.; Goings, J.; Peng, B.; Petrone, A.; Henderson, T.; Ranasinghe, D.; Zakrzewski, V. G.; Gao, J.; Rega, N.; Zheng, G.; Liang, W.; Hada, M.; Ehara, M.; Toyota, K.; Fukuda, R.; Hasegawa, J.; Ishida, M.; Nakajima, T.; Honda, Y.; Kitao, O.; Nakai, H.; Vreven, T.; Throssell, K.; Montgomery, J. A., Jr.; Peralta, J. E.; Oligaro, F.; Bearpark, M. J.; Heyd, J. J; Brothers, E. N.; Kudin, K. N.; Staroverov, V. N.; Keith, T. A.; Kobayashi, R.; Normand, J.; Ragavachari, K.; Rendell, A. P.; Burant, J. C.; Iyengar, S. S.; Tomasi, J.; Cossi, M.; Millam, J. M.; Klene, M.; Adamo, C.; Cammi, R.; Ochterski, J. W.; Martin, R. L.; Morokuma, K.; Farkas, O.; Foresman, J. B.; Fox, D. J. *Gaussian 16*, revision C.01; Gaussian, Inc.: Wallingford, CT, 2016.
(59) Weigend, F.; Ahlrichs, R. Balanced basis sets of split valence, triple zeta valence and quadruple zeta valence quality for H to Rn: Design and assessment of accuracy. *Phys. Chem. Chem. Phys.* **2005**, *7* (18), 3297−3305.
(60) Zheng, J.; Xu, X.; Truhlar, D. G. Minimally augmented Karlsruhe basis sets. *Theor. Chem. Acc.* **2011**, *128* (3), 295−305.
(61) Møller, C.; Plesset, M. S. Note on an Approximation Treatment for Many-Electron Systems. *Phys. Rev.* **1934**, *46* (7), 618−622.
(62) Vydrov, O. A.; Scuseria, G. E. Assessment of a long-range corrected hybrid functional. *J. Chem. Phys.* **2006**, *125* (23), 234109.
(63) Iikura, H.; Tsuneda, T.; Yanai, T.; Hirao, K. A long-range correction scheme for generalized-gradient-approximation exchange functionals. *J. Chem. Phys.* **2001**, *115* (8), 3540−3544.
(64) Chai, J.-D.; Head-Gordon, M. Long-range corrected hybrid density functionals with damped atom−atom dispersion corrections. *Phys. Chem. Chem. Phys.* **2008**, *10* (44), 6615−6620.
(65) Becke, A. D. A new mixing of Hartree-Fock and local density-functional theories. *J. Chem. Phys.* **1993**, *98* (2), 1372−1377.
(66) Grimme, S.; Antony, J.; Ehrlich, S.; Krieg, H. A consistent and accurate ab initio parametrization of density functional dispersion correction (DFT-D) for the 94 elements H-Pu. *J. Chem. Phys.* **2010**, *132* (15), 154104.
(67) Adamo, C.; Barone, V. Toward reliable density functional methods without adjustable parameters: The PBE0 model. *J. Chem. Phys.* **1999**, *110* (13), 6158−6170.
(68) Pople, J. A.; Krishnan, R.; Schlegel, H. B.; Binkley, J. S. Electron correlation theories and their application to the study of simple reaction potential surfaces. *Int. J. Quantum Chem.* **1978**, *14* (5), 545−560.
(69) Purvis, G. D., III; Bartlett, R. J. A full coupled-cluster singles and doubles model: The inclusion of disconnected triples. *J. Chem. Phys.* **1982**, *76* (4), 1910−1918.
(70) Boys, S. F.; Bernardi, F. The calculation of small molecular interactions by the differences of separate total energies. Some procedures with reduced errors. *Mol. Phys.* **1970**, *19* (4), 553−566.
(71) Groom, C. R.; Bruno, I. J.; Lightfoot, M. P.; Ward, S. C. The Cambridge Structural Database. *Acta Crystallogr. Sect. B* **2016**, *72* (2), 171−179.

https://doi.org/10.1021/acs.jpclett.5c02817
J. Phys. Chem. Lett. 2025, 16, 11064−11073

(72) Macrae, C. F.; Sovago, I.; Cottrell, S. J.; Galek, P. T. A.; McCabe, P.; Pidcock, E.; Platings, M.; Shields, G. P.; Stevens, J. S.; Towler, M.; Wood, P. A. Mercury 4.0: from visualization to analysis, design and prediction. *J. Appl. Crystallogr.* **2020**, *53* (1), 226−235.
(73) Humphrey, W.; Dalke, A.; Schulten, K. VMD: Visual molecular dynamics. *J. Mol. Graphics* **1996**, *14* (1), 33−38.

https://doi.org/10.1021/acs.jpclett.5c02817
J. Phys. Chem. Lett. 2025, 16, 11064−11073